NANO LETTERS

2008
Vol. 8, No. 5
1434-1438

Three-Dimensional Architecture of Inorganic Nanoarrays Electrodeposited through a Surface-Layer Protein Mask

Daniel B. Allred,[†,‡] Anchi Cheng,[†,§] Mehmet Sarikaya,[‡,||] François Baneyx,[‡] and Daniel T. Schwartz*[,‡,||]

Departments of Chemical Engineering and Materials Science and Engineering, University of Washington, Seattle, Washington 98195, and National Resource for Automated Molecular Microscopy, Department of Cell Biology, The Scripps Research Institute, La Jolla, California 92037

Received February 4, 2008

ABSTRACT

Transmission electron microscopy was used to analyze the three-dimensional (3D) architecture of cuprous oxide electrochemically deposited through the pores of the hexagonally packed intermediate surface-layer protein from *Deinococcus radiodurans* SARK. Imaging at multiple tilt angles and averaging from five different samples allowed ~3 nm computed 3D reconstructions of the inorganic deposit and protein template. We show that the electrodeposition process used here was able to fully access the pore structure that penetrates the protein layer, allowing the fabrication of a polycrystalline nanoarray with 18 nm periodicity and lateral interconnectivity among the pores with 3-fold symmetry. At the resolution of the reconstruction, the 6-fold symmetry pores also appear filled but are not connected laterally to the rest of the deposit. These results show that electrochemical deposition can produce interconnected 3D structures at dimensions an order of magnitude smaller than the most advanced integrated circuits (IC), boding well for continued down-scaling of electrodeposition to meet the needs for future generations of IC device interconnects.

For nanoscale systems, geometric details matter. Accurate three-dimensional (3D) control of the size, shape, interconnectivity, and organization of matter plays a crucial role in virtually all nanomaterial physical and chemical properties.[1–4] The characterization of complex 3D periodic architectures formed by liquid crystals, block copolymers, and crystallized proteins is normally accomplished using reciprocal space scattering experiments,[5,6] though it is becoming more common to directly image the 3D structure of proteins, virus, and fabricated systems, including their internal features, using advanced transmission electron microscopy (TEM) imaging and reconstruction methods.[7–9]

Previously, we demonstrated that 2D crystalline bacterial surface-layer (S-layer) proteins could be combined with electrodeposition to fabricate extremely high density ($>10^{12}$ cm^{-2}) metal and semiconductor nanoarrays.[10,11] Plan-view TEM analysis showed that the arrays produced by this fabrication strategy bore the symmetry and lateral spacing of the pores in the protein sheets. However, pores in S-layer proteins can follow tortuous paths and exhibit complex lateral interconnectivity.[12] Full 3D imaging of electrodeposited materials grown through a S-layer protein offers potential insights into the nature of solvent and ion accessibility in the protein pore network and provides information on how the protein sits on the surface. Technologically, electrodepositing a 3D network of inorganic material through a "mask" (the protein) with sub-10-nm lateral and transverse "lines" and "vias" will be the first demonstration that the critical dimensions of electrodeposited interconnects can be 10-fold smaller than currently found in advanced integrated circuits. Here we use 3D TEM methods to examine the structure of electrodeposited cuprous oxide grown through the hexagonally packed intermediate layer (HPI-layer) protein from *Deinococcus radiodurans*.

The HPI-layer protein was extracted from *D. radiodurans* using 2–5% sodium dodecyl sulfate treatment followed by repeated rinsing and differential centrifugation to remove bulk cell material and contaminating proteins loosely associated with hexagonally ordered HPI-layer protein "sheets".[11] Substrates were typically coated from a 0.25–1.0 mg mL^{-1} stock solution of protein by allowing a 2–3 μL droplet to contact the surface for 30–60 s and performing gentle rinsing. The atomic force microscopy (AFM) image of Figure 1A shows the 2D crystallinity of HPI-coated

* Corresponding author: dts@u.washington.edu.
† Daniel B. Allred and Anchi Cheng were equal contributors to this work.
‡ Department of Chemical Engineering, University of Washington.
§ National Resource for Automated Molecular Microscopy, Department of Cell Biology, The Scripps Research Institute.
|| Department of Materials Science and Engineering, University of Washington.

10.1021/nl0803444 CCC: $40.75
Published on Web 04/01/2008

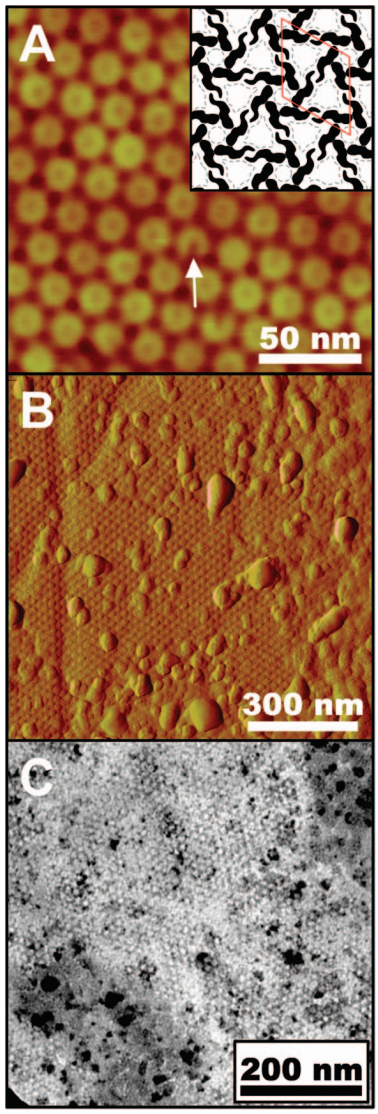

Figure 1. AFM and TEM images of the HPI-layer protein monolayer and of the electrodeposited structures. (A) AFM image showing that the HPI-layer consists of repeating hexamers (inset) that define an array of ~2 nm openings with 6-fold symmetry, and larger (~6 nm) openings with 3-fold symmetry. The arrow points to a single missing protomer. (B) Low-resolution AFM image acquired after electrodeposition of cuprous oxide through the HPI-layer mask. Electrodeposition was used to fill the structure, but nonuniformity leads to some overgrown areas. (C) TEM image showing that the deposition procedure fills most of the HPI layer. Overfilled regions can also be seen.

substrates prepared in this manner. Defects in the hexameric protein structure (inset) are rare and normally consist of an occasional missing monomer (arrow). Under typical preparation conditions, the 1–2 μm crystalline domains cover 40−80% of the substrate area. The plan-view inset and AFM image also show the two different hexagonal pore sublattices, one of which exhibits 3-fold symmetry and the other 6-fold symmetry.

Cuprous oxide (Cu_2O) was selected for templated electrodeposition experiments because it is an interesting semiconductor with multiple exciton adsorption bands in the visible spectrum[13,14] and because it can be deposited at sufficiently high nucleation densities to uniformly fill the sub-10-nm-sized HPI protein pores.[10,11] Panels B and C of Figure 1 show AFM and TEM images, respectively, after Cu_2O potentiostatic deposition at a potential of –450 mV vs saturated calomel electrode and in an electrolyte consisting of 0.4 M cupric and 3.0 M lactic acid adjusted to pH 9.0 with sodium hydroxide.[15] The topography revealed in the AFM image (Figure 1B) exhibits the expected hexagonal symmetry with deposited material having broken through and grown over the protein sheet on approximately one-third of the area. Such deposit overgrowth is necessary to ensure that the cuprous oxide thoroughly fills the protein mask. Transmission electron microscopy (TEM) provides complementary information to AFM, although it requires an electron transparent conducting substrate with surface properties that promote high nucleation densities. This was accomplished by adsorbing the HPI-layer proteins onto platinum-coated 400-mesh gold TEM grids, where the thin ~2 nm platinum film acts as both an electron transparent support film and an electrode for deposition of cuprous oxide through the protein mask, eliminating sample preparation prior to introduction into the electron microscope.[16] The transmitted electron image (Figure 1C) displays contrast due to the difference in electron density between the protein (low density, light) and cuprous oxide (high density, dark), as well as diffraction contrast due to the randomly oriented crystallites in the cuprous oxide. At the resolution shown, the hexagonal structure of deposit grown through the protein 3-fold sites is easily observed. Random dark regions are due to Cu_2O overgrowth of the protein or diffraction contrast from specific crystallite orientations. Regions of the image that do not display the hexagonal structure of the protein (e.g., the upper right corner of Figure 1C) are bare substrate where the cuprous oxide grows as a continuous thin film. We find that the best TEM imaging occurs when the protein nanomask is overfilled to a level comparable to that shown in Figure 1B.

TEM images acquired at multiple sample tilt angles, and from multiple protein regions, were used to reconstruct the 3D structure of the cuprous oxide deposit. Figure 2 shows several sample TEM images taken at different tilt angles, as well as the fast Fourier transform (FFT) reciprocal space representation of the –8° data (near-normal imaging). The images in Figure 2 have all been Fourier filtered, boxed, and lattice-straightened to accentuate the periodic structure, improve the signal, and attenuate random contrast features that arise from overfilling and diffraction contrast. The FFT data (shown, and others not shown) indicate an imaging resolution of approximately 3 nm. TEM imaging occurred with the angular distribution shown in Figure 3.

Correlation averaging from five different protein nanomask regions was used to reconstruct the average 3D electron density map for a particular sample. Figure 4 shows two representions of the 3D electron density data: as a 2D plot of the electron density variation for a selected plane through the 3D data (top of figure) or as 3D surface images showing the boundaries of a selected electron density contour as seen from a chosen viewing angle (below in figure). The electron

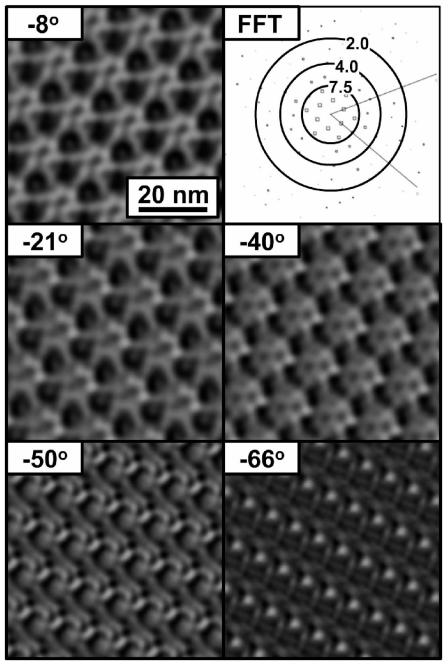

Figure 2. Representative TEM tilt series for electrodeposited cuprous oxide (dark) grown through the HPI-layer protein (light) along one of two orthogonal tilt axes. Fourier filtered images of five different tilt angles and the fast Fourier transform (FFT) of the –8° tilt image are shown. Resolution rings in the FFT image (marked in nanometers) indicate that the resolution is ~3 nm.

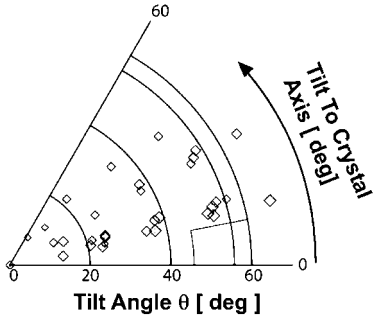

Figure 3. Tilt geometry and image quality plot of the sample. The tilt angle toward the vertical is shown along the *x*-axis and the angle with respect to the 6-fold axis is shown along the polar coordinate. Individual image quality is displayed as values ranking from 1 to 5. The size of the symbols is proportional to the significance of the data in the reconstruction; more detailed interpretation can found in the work of Cheng and Yeager.[17]

density map for the cross-section plane **A···A** through the sample thickness is shown at the top of Figure 4. The electron density map ranges from the lowest electron density regions (blue) to the highest electron density regions (deep red). Three regions, denoted i, ii, and iii, can be identified in the electron density map cross section. Region i corresponds to the ~2 nm ultrathin platinum film onto which HPI proteins were adsorbed. Region ii is a roughly 7 nm thick zone where protein monolayer and cuprous oxide coexist, while region iii is the layer where overfilling of the protein occurs. The latter region appears to be laden with reconstruction artifacts, probably because only part of the sample is overgrown with

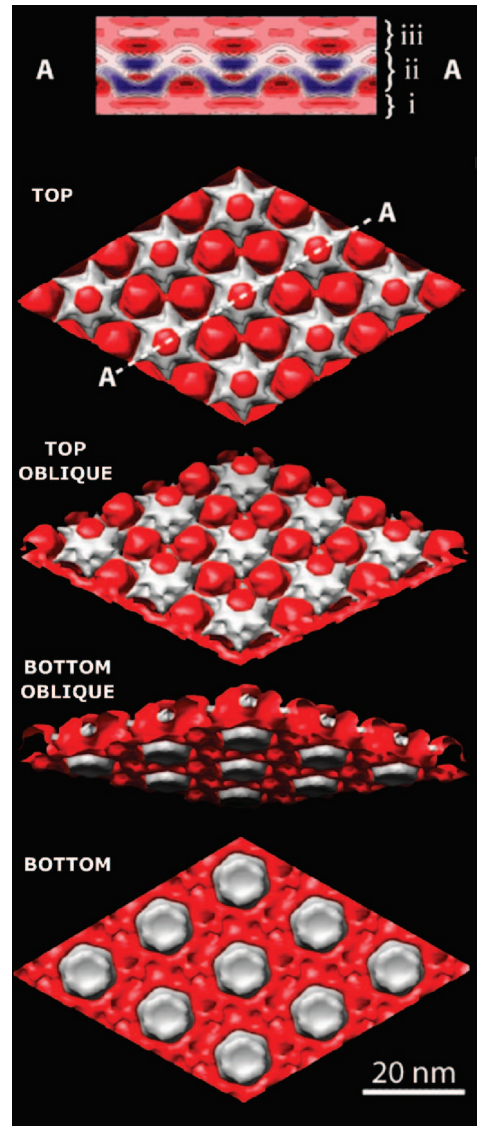

Figure 4. Several views of the 3D reconstruction showing electron density contours representing cuprous oxide (red) and protein (white). The viewing angle progresses from the electrolyte side of the sample (top) to the substrate side (bottom). The full electron density map is shown for the cross section **A···A**, with labeled regions indicating (i) the substrate, (ii) the protein/inorganic nanocomposite, and (iii) the overgrowth above the protein at the top. Resolution ≈ 3 nm.

cuprous oxide as seen in topography data such as shown in Figure 1B.

By selection of a single red and a single white electron density contour line from the electron density map, 3D surface plots were generated to visualize the boundary between cuprous oxide (red) and protein (white). Starting from the first surface-rendered image of Figure 4 and working down, one sees surface plots of region ii viewed progressively from the top (electrolyte side) to the bottom (substrate side) of the sample. At the resolution of the reconstruction, single protomers are not visible, but the hexameric nature of the protein monolayer is quite clear, as is its chirality. The top view shows that both 3-fold pores and 6-fold pores are solvent and ion accessible (a requirement for electrodeposition) and that larger diameter pillars of

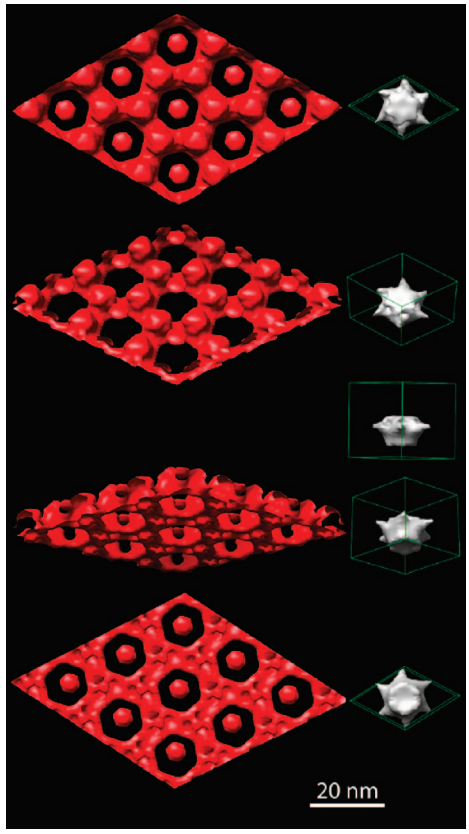

Figure 5. Viewing the inorganic (red) and hexameric protein unit (white) separately reveals details of the 3D architecture of both. At the 3 nm resolution of these studies, the protein hexamer matches higher resolution 3D reconstructions of the HPI-layer protein, indicating that the electrodeposited material (the contrast agent here) produced a high fidelity negative replica of the protein.

cuprous oxide grow through the 3-fold pores relative to the 6-fold pores. In plan-view TEM (Figure 1C), the particles produced through 3-fold pores appear to be isolated from one another. However, observation in three-dimensions with the protein removed (Figure 5), shows that the nanoarray of cuprous oxide particles produced by the 3-fold pores is an interconnected latticework that grows beneath the connecting spiral arms of the hexameric units. In the surface plots of Figure 5, the cuprous oxide array templated by the 6-fold pores appears to be sitting on top of the protein, without continuous connection to the substrate. Similarly, the **A···A** electron density map cross section (Figure 4) only shows cuprous oxide on top and in the middle of the 6-fold pore. Since the size of the 6-fold pore and the resolution of our reconstruction are both near 3 nm, the lack of a clear electronically conducting path to the substrate is likely to be a reconstruction artifact. However, these length scales are approaching those where tunneling or protein-mediated charge transfer are possible. Whether or not the latter is at play is difficult to assess since the structure of the HPI-layer protein has not been solved and the identity of the residues lining the 6-fold pore is unknown.

Figure 5 separates the surface plots from Figure 4 to more clearly show the 3D network of electrodeposited cuprous oxide and the protein structure. At the accelerating voltages used here, the low electron density protein is nearly invisible to the TEM beam, so the hexameric protein unit shown in Figure 5 represents the negative structure (e.g., the regions where cuprous oxide did not electrodeposit). Traditional negative staining methods have previously been used to determine the electron density map for of the HPI-layer protein.[18] The structure of the hexamer shown in Figure 5 matches quite well with these data, lending credibility to our reconstruction data and indicating high fidelity of the electrodeposition process. Several features of the electrodeposited cuprous oxide structures of Figure 5 are worthy of comments. The continuous hexagonal lattice of cuprous oxide adjacent to the substrate is ~3 nm thick, and passes beneath the raised portions of the protomers that interconnect to form self-assembled S-layer sheets.[18] Since electrodeposition proceeds from the substrate outward, the hexagonal lattice is likely to be the first part of the structure to be completed during the initial phases of growth. As electrodeposition continues, the cuprous oxide will fill the 3-fold pores and form the (somewhat indeterminate) cuprous oxide structures seen in the 6-fold pores. Overall, it appears that the entire protein structure is fully solvent and ion accessible. This suggests that the amino acids that line the walls of the pores have a hydrophilic character and are not highly charged at the pH of 9.0 used for electrodeposition, although more careful charge-screening studies have not yet been carried out.

The continuously interconnected lattice and vertical pillars observed in the three-dimensional TEM reconstructions resemble the lines and vias seen in electrodeposited copper interconnects for state-of-the-art integrated circuits (ICs). However, the interconnect networks we demonstrate here are formed at an areal density several orders of magnitude greater than that manufactured by photolithography at the time of this writing. Our ability to demonstrate 3D electrodeposited networks augurs well for the future scalability of electrodeposition through future IC device generations.[19]

Acknowledgment. This work was supported by the National Science Foundation IGERT (9987620), NNIN (0335765), and MRSEC (0520567) programs, and the Boeing-Sutter Endowment for Excellence in Engineering. Some of the work was conducted at the National Resource for Automated Molecular Microscopy which was supported by the National Institutes of Health through the National Center for Research Resources P41 program (RR17573).

References

(1) Hartland, G. V. *Annu. Rev. Phys. Chem.* **2006**, *57*, 403.
(2) Sherry, L. J.; Jin, R.; Mirkin, C. A.; Schatz, G. C.; Van Duyne, R. P. *Nano Lett.* **2006**, *6*, 2060.
(3) Wiley, B. J.; Im, S. H.; Li, Z.-Y.; McLellan, J.; Siekkinen, A. R.; Xia, Y. *J. Phys. Chem. B* **2006**, *110*, 15666.
(4) Petrova, H.; Lin, C.-H.; Hu, M.; Chen, J.; Siekkinen, A. R.; Xia, Y.; Sader, J. E.; Hartland, G. V. *Nano Lett.* **2007**, *7*, 1059.
(5) Koch, C. T. *Mater. Sci. Eng., A* **2006**, *422*, 41.
(6) Zuo, J. M.; Vartanyants, I.; Gao, M.; Zhang, R.; Nagahara, L. A. *Science* **2003**, *300*, 1419.
(7) Nickell, S.; Förster, F.; Linaroudis, A.; Del Net, W.; Beck, F.; Hegerl, R.; Baumeister, W.; Plitzko, J. M. *J. Struct. Biol.* **2005**, *149*, 227.
(8) Nickell, S.; Park, P. S.-H.; Baumeister, W.; Palczewski, K. *J. Cell Biol.* **2004**, *177*, 917.

(9) Kohjiya, S.; Katoh, A.; Shimanuki, J.; Hasegawa, T.; Ikeda, Y. *Polymer 2005* **2005**, 4440.
(10) Allred, D. B.; Sarikaya, M.; Baneyx, F.; Schwartz, D. T. *Nano Lett.* **2005**, *5*, 609.
(11) Allred, D. B.; Sarikaya, M.; Baneyx, F.; Schwartz, D. T. *Electrochim. Acta* **2007**, *53*, 193.
(12) Engelhardt, H.; Peters, J. *J. Struct. Biol.* **1998**, *124*, 276.
(13) Rakhshani, A. E. *Solid-State Electron.* **1986**, *29*, 7.
(14) Kavoulakis, G. M.; Baym, G. *Phys. Rev. B* **1996**, *54*, 16625.
(15) Zhou, Y.; Switzer, J. A. *Scr. Mater.* **1998**, *38*, 1731.
(16) Allred, D. B.; Zin, M. T.; Ma, H.; Sarikaya, M.; Baneyx, F.; Jen, A. K.-Y.; Schwartz, D. T. *Thin Solid Films* **2007**, *515*, 5341.
(17) Cheng, A.; Yeager, M. *Acta Crystallogr., Sect. A* **2004**, *60*, 351.
(18) Baumeister, W.; Barth, M.; Hegerl, R.; Guckenberger, R. *J. Mol. Biol.* **1986**, *187*, 241.
(19) Haensch, W.; Nowak, E. J.; Dennard, R. H.; Solomon, P. M.; Bryant, A.; Dokumaci, O. H.; Kumar, A.; Wang, X.; Johnson, J. B.; Fischetti, M. V. *IBM J. Res. Dev.* **2006**, *50*, 339.

NL0803444